Postprint of: Wilczewska P., Bielicka-Giełdoń A., Fiszka Borzyszkowska A., Ryl J., Klimczuk T., Siedlecka E. M., Photocatalytic activity of solvothermal prepared BiOClBr with imidazolium ionic liquids as a halogen sources in cytostatic drugs removal, Journal of Photochemistry and Photobiology A: Chemistry, Vol. 382 (2019), 111932, DOI: 10.1016/j.jphotochem.2019.111932

Photocatalytic activity of solvothermal prepared BiOClBr with imidazolium ionic liquids as a halogen sources in cytostatic drugs removal

Patrycja Wilczewska[1], Aleksandra Bielicka-Giełdoń[1*], Agnieszka Fiszka Borzyszkowska[1], Jacek Ryl[2], Tomasz Klimczuk[3], Ewa Maria Siedlecka[1]

[1]Faculty of Chemistry of the University of Gdansk, Wita Stwosza 63, 80-308 Gdansk

[2]Faculty of Chemistry of the Gdansk University of Technology, Gabriela Narutowicza 11/12, 80-233 Gdansk

[3]Faculty of Applied Physics and Mathematics, Gdansk University of Technology, Gabriela Narutowicza 11/12, 80-233 Gdansk

Corresponding author. E-mail address: a.bielicka-gieldon@ug.edu.pl

ABSTRACT

In this work, the BiOClBr, as a new family of bismuth based semiconductors, was successfully applied to remove of cytostatic drugs from water under UV-Vis light irradiation. BiOCl, BiOBr and BiOClBr were synthesized using two steps solvothermal method in glycerol. The inorganic salts (KCl and KBr) and 1-butyl-3-metylimidazolium chloride (BmimCl) and 1-butyl-3-metylimidazolium bromide (BmimBr) ionic liquids (ILs) were used as the source of halides for the photocatalysts synthesis. The as-fabricated samples were characterized by X-ray diffraction (XRD), X-ray photoelectron spectroscopy (XPS), scanning electron microscopy (SEM) and UV-vis diffuse reflectance spectroscopy (DRS). The specific surface area was measured by Brauner-Emmett-Teller (BET) technique. Additionally, Fourier-transform infrared spectroscopy was used to evaluate the presence of IL on the photocatalysts surface. The comparison of photocatalytic activity between BiOCl and BiOClBr photocatalysts towards 5-fluorouracil (5-FU), imatinib (IMA) and cyclophosphamide (CP) removal was conducted. The

highest photocatalytic activity in the cytostatic drugs degradation and mineralization was found using BiOClBr IL synthetized via ILs as the halogens source. The study showed that BiOClBr IL synthesized in the presence of ILs can be a promising material in the water decontamination methods.

Keywords: BiOClBr, photocatalysis, ionic liquids, synthesis, cytostatic drugs

1. INTRODUCTION

Pharmaceutical and personal care products (PPCPs) have attracted significant concerns worldwide for their persistence and potential threat to the ecosystem and public health [1]. They are commonly present in water at concentrations ranging from a few ng L^{-1} to several μg L^{-1}. Cytostatic drugs are a broad group of chemotherapy compounds mainly applied in medication for tumor, skin diseases and infections treatments [2]. These drugs and their human metabolites can directly enter into the water cycle from the hospital effluent, household and industrial wastewater, and drug waste disposal [2-5]. They exhibit carcinogenic, mutagenic and teratogenic activity and also have been recognized as low biodegradable and chemically unstable substances [3]. Due to these properties, cytostatic drugs are not completely removal by conventional wastewater treatment plants (WWTPs) [6-8]. They are continuously discharged to the environment with the effluents from WWTPs, and the accumulation of these drugs become a threat to ecosystem and living organisms [9-10]. Their removal is also a challenge for the water purification methods. Therefore, an effective treatment processes for these classes of substances is urgently needed in both scientific and industrial applications.

Photocatalytic oxidation is one of the most promising advanced oxidation technologies (AOTs) able to the mineralization of persistent contaminants. The bismuth-based photocatalysis presents probably the most promising approach in terms of low toxicity of semiconductor and the availability of substrates for its preparation process. Bismuth oxyhalides (BiOX, X=Cl, Br,

I) are V-VI-VII ternary semiconductors compound with tetragonal matlockite structure, a layer structure characterized by $[Bi_2O_2]^{2+}$ slabs inserted between double slabs of halogen atoms. The engineering techniques such as microstructure modulation, heterologous hybridization and structural design of BiOX for efficient photocatalytic applications is crucial and attracts the attention of many research groups [11-13]. BiOClBr is a new family of bismuth semiconductors. It was reported that this family of photocatalysts exhibited a high photocatalytic activity under visible light toward dyes removal [14-16].

Ionic liquids (ILs), usually composed of asymmetric organic cations and large inorganic anions have attracted much attention as functional materials for controllable synthesis of nanostructures. They can act as a templates leading to unusual morphology of different materials [17-18], and they can be a source of halide atoms in BiOX preparation. Reported research showed that using IL as a halogen source in solvothermal synthesis resulted in more crystalized BiOCl [19], BiOBr [20], $Bi_4O_5Br_2$ [21] photocatalysts when compared to inorganic salts. BiOClBr with good photocatalytic activity was obtained via solvothermal method under temperature 140°C for 24h. The ethylene glycol was used as a solvent, while 1-hexadecyl-3-methylimidazolium chloride/bromide (C_{16}mimCl/Br) was a source of halogens in reaction [22, 23]. Alternative synthesis was proposed by Li at al., BiOCl/BiOBr were prepared in the solvothermal reaction with C_{16}mimCl/Br in 0.1M mannitol in the 140°C for 24h [15]. As the halogen source in bismuth oxyhalides BiOX (X=Cl, Br, I) synthesis C_{12}mimCl/Br/I [24], C_8mimCl [19], C_6mimCl/Br [24] and BmimCl/Br/I were applied [19-20, 24]. Solvothermal reaction were examined in a range of temperatures from 140°C to 180°C and throughout a varied time ranging from 6h to 24h ethylene glycol or 2-metoxyethanol was used as a solvent.

To our best knowledge, there is no comparative study of photocatalytic activity of BiOXY solid solutions prepared by the solvothermal method with the BmimX ionic liquids used as the halogen ions precursors.

In this study a series of BiOX and BiOXY (X,Y=Cl, Br) were prepared via solvothermal process, where the BmimX was used as a source of halide atoms. The effects of the ILs on photocatalytic activity under solar light of as-prepared BiOX and BIOXY were examined by degradation of cytostatic drugs such as: 5-fluorouracil, cyclophosphamide and imatinib. The studied drugs are considered harmful micropollutants exhibiting a cancerogenic activity.

The BiOClBr photocatalyst with the increased activity towards the cytostatic drugs with the different physicochemical properties and chemical structure was obtained. The results showed the photocatalytic degradation both of aromatic compound with the low adsorption properties (5-FU logKo/w=-0.89), aliphatic compound with chloride atoms (CF), and IMA – aromatic compound with relatively high adsorption possibility. Such a set of compounds with different physicochemical properties and significant biological activity was the first time studied with using BiOClBr photocatalyst. Not only the removal of model compounds from water but the mineralization efficiency was also considered. The adsorption and photocatalysis processes were studied in details. Kinetics and mechanistic studies including the identification of main active species contributing to the organic matter removal were also explored.

2. MATERIALS AND METHODS

Bismuth nitrate, 1-butyl-3-methylimidazolium chloride (BmimCl) and bromide (BmimBr), potassium chloride and bromide, glycerol were purchased from StanLab Sp. J. Ethyl alcohol, chloroform, *tert*-butyl alcohol and sodium hydroxide were obtained from POCh S.A, while 5-fluorouracil, imatinib, cyclophosphamide, *p*-benzoquinone, nitrotetrazolium blue chloride, terephalic acid and acetonitrile HPLC grade were purchased from Sigma-Aldrich. L-(+) ascorbic acid was from Chempur® and Na_2EDTA dehydrate was provided from Acros Organics. All reagents were used in analytical grade and without further purification.

2.1. Synthesis of BiOCl(Br)

The BiOCl, BiOBr and BiOClBr photocatalysts were synthesized in glycerol using two steps solvothermal method. In typical synthesis, 8 mmol $Bi(NO_3)_3 \cdot 5H_2O$ was dissolved completely in 80 mL of glycerol to obtain the homogenous solution A and 8 mmol KCl (8 mmol KBr for BiOBr or 4 mmol KCl and 4 mmol KBr for BiOClBr) was dissolved in 80 mL of glycerol to obtained the solution B. Solution B was added by drops to solution A with magnetic stirring at a room temperature. After further stirring for 30 minutes, the mixture was transferred into 200 mL Teflon-lined stainless steel autoclave, which was sealed and maintained at 160˚C for 16 h and then cooled to room temperature [25]. The obtained complex precursor was washed with ethyl alcohol several times and then dried under air at 80°C for 12 h. The studied photocatalysts were obtained via hydrolytic process from an aqueous solution of their complex precursor molecules. 100 mL of distilled water was added to every 0.3 g of precipitate. The suspension was continuously stirred at a room temperature for 2 h, and the powder was filtered and washed with distilled water. Finally, the photocatalyst was dried under the same conditions as previously obtained precipitate. The samples prepared using the method were identified as BiOCl, BiOBr and BiOClBr. Further BiOCl(Br) photocatalysts were synthesized via ionic liquids (ILs). The BmimCl and/or BmimBr were used as a halides sources instead of inorganic salts KCl or KBr. The photocatalysts prepared in reaction with BmimX were labeled as BiOCl IL, BiOBr IL and BiOClBr IL. The molar ratio of Cl/Br used to synthesis of BiOClBr and BiOClBr IL was 1:1.

2.2 Characterization of BiOCl(Br) and BiOCl(Br) IL

The X-ray diffraction technique (XRD) was used to identify the crystalline structure of photocatalysts with PANalytical X'Pert Plus diffractometer with focusing primary monochromator CuKα (λ = 1.54 Å) radiation. The morphology and microstructure of samples were investigation by field emission scanning electron microscopy with JEOL JSM-7610F FE-SEM. The optical properties was analyzed using UV–vis diffuse reflectance spectra (DRS)

which were obtained by 2600 UV-VIS Spectrophotometer Shimadzu. $BaSO_4$ was used as a reference. The photoluminescence spectrum (PL) was obtained by Perkin Elmer limited LS50B spectrophotometer in the range of 300–700 nm. The excitation wavelength was 315 nm, while the emission was detected up to 390 nm. Fourier transform-infrared (FT-IR) spectra were measured on a Bunker IFS66 spectrophotometer in the range 4600-400 cm^{-1} using KBr pellet technique. The Brunauer-Emmett-Teller (BET) specific surface areas of the samples were analysed by nitrogen adsorption using a Micromeritics Gemini V (model 2365) nitrogen adsorption apparatus. X-ray photoelectron spectroscopy with ThermoFisher Scientific Escalab 250Xi was used to determine the composition of the photocatalysts surface.

The pH_{zpc} (point of zero charge) of samples determination was performed in 0.01 M NaCl with different pH in the range between 2 and 12 adjusted by HCl or NaOH solution. 20 mg of photocatalyst was added to 5 mL of 0.01 M NaCl with appropriate pH values [26]. The flasks with mixture were rapidly stirred for 24h and subsequently the final pH of the solution was measured by pHmeter CyberScan Ion510. A graphs were plotted between pH_{final} vs $pH_{initial.}$ The point of intersection of those pH curves was recorded as pH_{zpc} in function of the photocatalysts surface.

2.3 Photocatalytic activity

Photocatalytic degradation of cytostatic drugs: 5-fluorouracil (5-FU), cyclophosphamide (CP) and imatinib (IMA) in the presence of BiOCl(Br) and BiOCl(Br) IL were conducted under a 150 W Heraeus medium-pressure mercury lamp irradiation. Photocatalytic tests were performed for 120 minutes. In the experiment 3 mg (0.5 g L^{-1}) of photocatalyst was dispersed into 15 mL of 5-FU, CP and IMA solution with the initial concentration of 15 mg L^{-1}. Before starting the irradiation, the contaminants and photocatalyst displayed adsorption-desorption equilibrium by being stirred continuously for 30 minutes. The experimental conditions were previously optimized based on the 5-FU. At prearranged times intervals 1 mL of suspensions

samples were filtered through 0.22 μm syringe filters to eliminate photocatalyst particles from the sample. The concentration of drugs in the samples were examined by HPLC technique. The physical and chemical properties of cytostatic drugs applied are listed in Table 1.

Table 1. Physical and chemical properties of cytostatic drugs.

Name	Chemical structure	Chemical character	pKa	$LogK_{o/w}$	Ref.
5-Fluorouracil (5-FU)	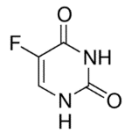	aromatic compound, weakly adsorbed species	pKa_1=7.5 pKa_2=9.0	-0.89	[26-27]
Cyclophosphamide (CP)	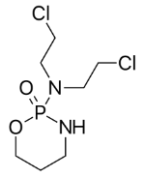	aliphatic compound, weakly adsorbed species	pKa_1=2.3 pKa_2=11.1	0.63	
Imatinib (IMA)	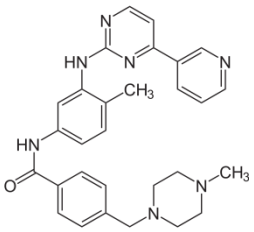	aromatic compound, adsorbed species	pKa_1=8.07 pKa_2=3.73 pKa_3=2.56 pKa_4=1.52	2.89	

2.4. *Identification of photogenerated entities*

Chloroform, *tert*-butyl alcohol, *L*-ascorbic acid and disodium ethylenediaminetetraacetate dihydrate (Na_2EDTA) in amount of 10 mM were used in the described photocatalytic process as a scavengers of electrons (e^-), hydroxyl radicals ($^{\bullet}OH$), superoxide radical ($^{\bullet}O_2^-$) and holes (h^+), respectively. The $^{\bullet}OH$ generation in the presence of fabricated samples was examined by analyzing the fluorescence intensity of a product of reaction between terephalic acid (TA) and hydroxyl radicals (2-hydroxyterephalic acid). In a typical process, 15 mg of photocatalyst is added to 75 mL of $2 \cdot 10^{-3}$ M NaOH solution containing $5 \cdot 10^{-5}$ M TA. The obtained solution was stirred in the dark for 30 min before solar light illumination (Suntest CPS+ solar simulator equipped with cooling system and 1700W Xenon lamp as the light source). 2 mL of sample

was collected at 30 minutes intervals during 1 h illumination of mixture and filtered off. A Perkin Elmer limited LS50B spectrophotometer was used to record the fluorescence spectra of samples in the range 300 – 700 nm. The excitation wavelength was 300 nm. In order to evaluate $^{\bullet}O_2^{-\bullet}$ generation in the presence of photocatalysts, the experiments with 4-Nitro blue tetrazolium chloride (NBT) were conducted. The concentration of NBT was $2.5 \cdot 10^{-5}$ M. The irradiations were carried out for 90 min in Suntest CPS+, taking 1.5 ml of the sample every 15 min and measure absorbance of NBT at 259 nm on Perkin Elmer Lambda XLS+.

2.5.*Analytical methods*

5-FU, CP and IMA concentration were determined with HPLC system with UV detector (Perkin Elmer, Series 200). The chromatographic conditions were listed in Table 2. Chromatographic column used in experiments was Phenomenex Kinetex C-18 column (150x4.6 mm, 2.6 μm).

Table 2. Analytical parameters drugs analysis.

Parameter	**5-FU**	**CP**	**IMA**
Detection wavelength [nm]	266	200	302
Flow rate [mL min^{-1}]	0.7	0.5	1.0
Injection volume [μm]	25	50	30
Analysis time [min]	6	10	7
Mobile phase	Acetonitrile/water 2:98 (v/v)	Acetonitrile/water 30:70 (v/v)	Acetonitrile/0.1% formic acid water solution 10:90 (v/v)

The progress of the mineralization of the 5-FU, CP and IMA was monitored by measuring the Total Organic Carbon (TOC) and Total Nitrogen via Total Organic Carbon analyzer, Total Nitrogen Measuring UNIT Shimadzu.

3. RESULTS AND DISCUSSION

3.1. XRD analysis

X-ray diffraction analysis of prepared photocatalysts was used to determine the purity and crystallinity of samples synthesised with an inorganic salts KCl/KBr or an ionic liquids BmimCl/BmimBr. The intensity of reflections and sharp diffraction peaks in Figure 1a and 1b indicated the well-crystallized structures of all samples. Precisely, the evolution of the three strongest peaks is shown in the enlarged XRD patterns (Fig. 1 cd).

The reflections observed for BiOCl IL were narrower and more intense than those found in diffraction pattern of BiOCl (ICCD 01-085-0861), indicating that the first set was better crystallized than second one. The results are in accordance with the previously reports showing, suggesting the BiOCl materials obtained via IL were well crystalized and high purity [19, 29-30]. In both cases, the samples were the pure BiOCl phase.

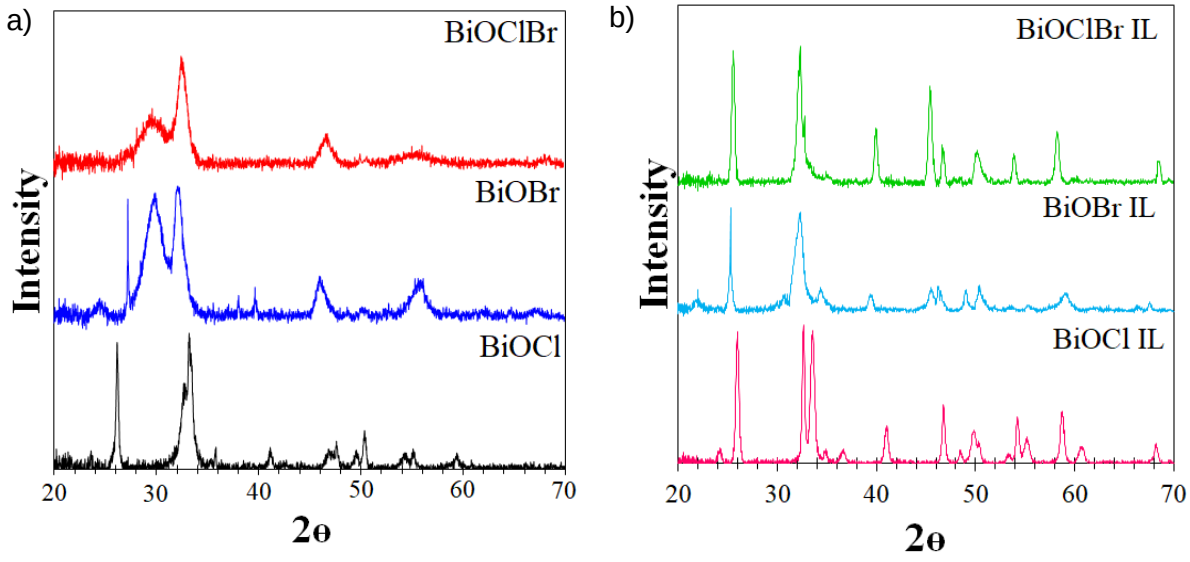

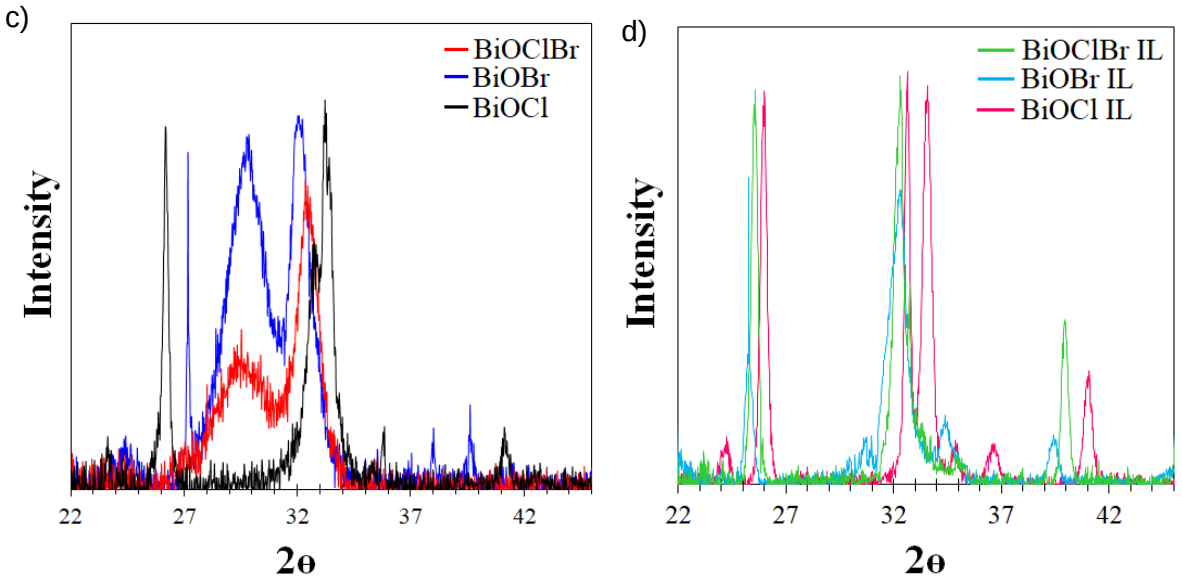

Figure 1. XRD patterns of synthesized photocatalysts a) with inorganic salts and b) ionic liquid as a halogen source and shifts of diffraction peaks in c) BiOClBr and d) BiOClBr IL in selected 2θ

The XRD pattern of BiOBr and BiOBr IL implied, that this studied samples were $Bi_4O_5Br_2$ (ICDD 01-071-3449) crystal phase. Synthesis bismuth oxybromide from KBr not allowed to obtained BiOBr phase in proposed conditions. Preparation this type photocatalysts via BmimBr resulted that BiOBr (ICCD 01-081-8953) phase was in residual amount and the main phase was $Bi_4O_5Br_2$. Moreover, the reflections and diffraction peaks broadening found for BiOBr and BiOBr IL indicated very small crystallites in both samples.

XRD pattern of a multicomponent sample BiOClBr shown in Fig 1b exhibited a diffraction peaks characteristic for the pure BiOCl (ICDD 01-085-0861) and BiOBr (ICDD 01-081-8953). The peaks broadening for samples BiOClBr prepared by the reaction with KCl/KBr were higher than those obtained for BiOBrCl IL. The used of BmimBr and BmimCl in fabrication of BiOClBr IL allowed to prepare the more crystalized material than BiOClBr. In BiOClBr IL photocatalyst bromine atoms (rBr^- = 0.196 nm) with large atom diameter incorporated into the

crystallographic lattice with chlorine atoms (rCl^{-} = 0.181 nm) with relatively low diameter. This phenomena was found as diffraction peaks shift in XRD pattern for the sample.

3.2. UV-vis diffuse reflectance spectroscopy

The UV-vis diffuse reflectance spectra (DRS) of the prepared photocatalysts are shown in Fig 2a. BiOCl and BiOCl IL mainly showed absorption in the UV region with absorption edge at around 350 nm as illustrated Fig 2a. Ability of light absorption in the visible region is marginal, but BiOCl IL had a slightly better absorption in this region than BiOCl [31]. The UV-vis/DRS spectra of BiOBr and BiOBr IL were characteristic for $Bi_4O_5Br_2$ crystal phase as it was found in XRD analysis [32-33]. BiOClBr absorbed light more intensively than BiOClBr IL in all regions.

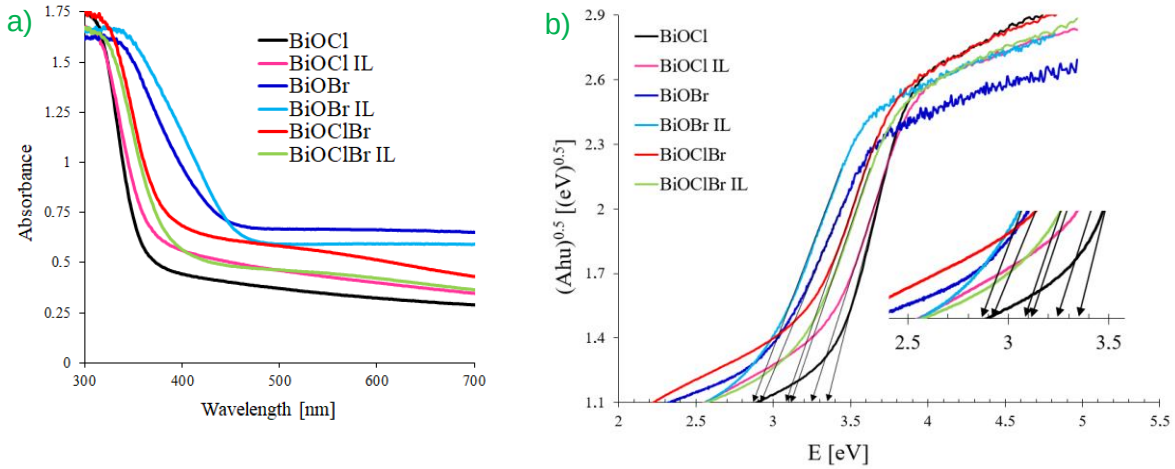

Fig. 2. a) UV-vis diffuse reflectance spectra of BIOXY and b) Kubelka-Munk transformation of prepared photocatalysts.

According to the DRS analysis after Kubelk-Munk transformation the band gaps of the BiOCl, BiOCl IL, BiOBr, BiOBr IL, BiOClBr and BiOClBr IL were respectively 3.35, 3.25, 2.86, 2.91, 3.08, 3.14 eV. Eg values were similar to that from literature reports [14-15, 31, 33-34]. Photocatalyst BiOCl fabricated with ILs were characterized by slightly better absorption and

narrower band gaps. This observation has been confirmed by other research groups [22-23, 35-37]. They showed that the Eg value of BiOCl prepared in reaction with KCl was slightly higher than that obtained for sample prepared with C_{16}mimCl. However, the introduction of bromine by BmimBr into BiOBr and BiOClBr caused the broaden of Eg [14]. To our best knowledge, up till now there have been any Bmim IL used to preparation of BiOBr and BiOClBr.

Table 1. Values of energy band gap, specific surface area (S_{BET}) and pore size.

Photocatalyst	**Eg [eV]**	**S_{BET} [$m^2\ g^{-1}$]**	**Total pore volume [cm^3/g]**
BiOCl	3.35	90.8	0.043
BiOCl IL	3.25	54.7	0.026
BiOBr	2.86	49.2	0.024
BiOBr IL	2.91	79.3	0.038
BiOClBr	3.08	65.6	0.032
BiOClBr IL	3.14	57.9	0.029

3.3. BET analysis

The specific surface area and pore average diameter of as prepared photocatalysts are listed in Table 1. In the literature, the specific surface areas of flower-like BiOCl were reported as 1.84 – 18.04 $m^2\ g^{-1}$ [37-40], while $Bi_4O_5Br_2$ formed structure 3D with specific surface area of 23.9 - 62.25 $m^2\ g^{-1}$ [24, 32, 41-42]. The surface of BiOClBr was synthesized by the solvothermal method under different conditions (solvent, temperature, synthesis time) and reported in the literature in the range of 2.01-14.16 [43-46]. In all cases, the surface of reported photocatalysts was much smaller than those obtained in this study. The large specific surface area and porosity were the result of the use of glycerol as a solvent in sample preparation, while the presence of ILs in synthesis increased (BiOCl IL) or decreased (BiOBr IL and BiOClBr IL) their values. The enhanced surface area and the appropriate pore size of photocatalysts can facilitate to the adsorption and transfer of pollutants molecules to active sites thus improving the photocatalytic efficiency.

3.4. *SEM analysis*

SEM images (Fig. 3ab) of BiOCl and BiOCl IL samples showed that they were microsphere-like. Both photocatalysts were built from several dozen of thin nanosheets, although, BiOCl IL sheets were less close-packed. This findings was confirmed by BET surface analysis (Table 1). BiOBr crystallites (Fig. 3cd) were composed of massive interleaving nanosheets but much thicker and with more blurry shapes than BiOBr IL. BiOBr IL nanoparticles were a flower-like shape with relatively high and thin nanosheets. The specific surface area of BiOBr IL sample was 1.6 times higher than BiOBr. Furthermore, BiOClBr and BiOClBr IL (Fig. 3ef) are hierarchical microspheres constructed by numerous two dimensional interlaced nanosheets with thickness of 10-20 nm and 5-15 nm for BiOClBr and BiOClBr IL, respectively.

The average diameters of photocatalyst particles were in the range of 0.5-1 (BiOBr), 1-1.8 (BiOCl IL), 1-2 (BiOCl), 1.4 – 1.89 (BiOClBr), 2.28 – 2.75 (BiOClBr IL) and 2.91 - 3.13 μm (BiOBr IL).

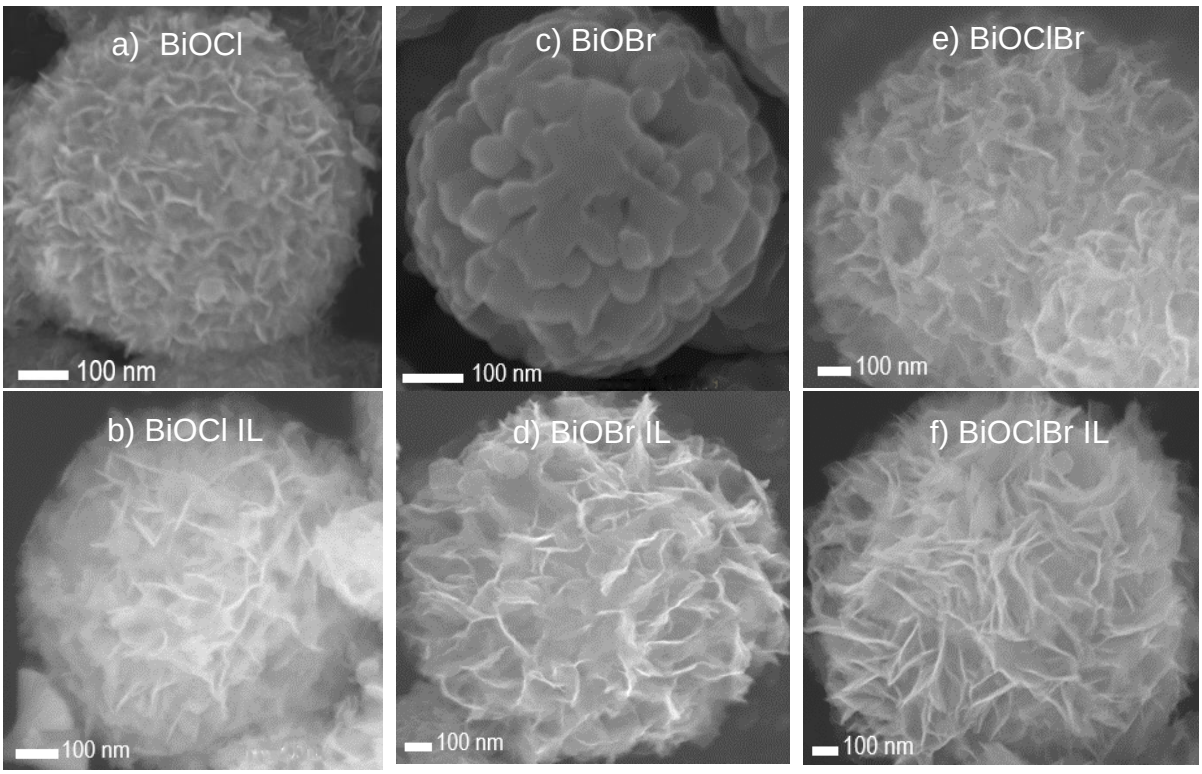

Fig. 3. SEM image of synthesized photocatalysts.

3.5. *FT-IR analysis*

In the Fig S3. the FT-IR spectra of samples obtained via KCl/KBr and ILs were presented. In the all spectrum of the as-prepared photocatalysts peaks corresponded to the bonds vibration associated with water molecules adsorbed (ca. 1380 cm^{-1}) and of the organic contaminants adsorbed on the surface of photocatalytic materials. A strong absorption band at *ca.* 530 cm^{-1} can be attributed to the Bi-O symmetric starched mode, which confirms the formation of BiOCl (BiOBr) [35-36, 47]. No characteristic peaks of imidazolium C-H stretching of the IL were observed in FT-IR spectra. It can be assumed that the ILs were completely removed from the surface of the material by washing with deionized water and alcohol. FT-IR analysis was consistent with the results obtained from XPS measurements.

3.6. *XPS analysis*

In order to investigated the surface composition and chemical states of BiOClBr and BiOClBr IL, X-ray photoelectron spectroscopy (XPS) measurement was performed. The survey in Fig 4a showed the presence of the Bi, O, Cl and Br peaks which confirmed the compositions of sample BiOClBr IL with the Cl/Br ratio of 1:1.

The peak for N 1s, typically located at 405 eV, was not observed. This suggests that ILs were completely removed from the surface of the studied sample. The same finding was observed for the other samples synthesized via ILs (BiOCl IL, BiOBr IL). In the Fig. 4b XPS spectra of Bi 4f regions from the surface of the BiOClBr IL was shown. In the high-resolution spectrum (Fig. 4b) two strong peaks at binding energies of around 165.2 eV and 158.7 eV were assigned to the Bi $4f_{7/2}$ and Bi $4f_{5/2}$ respectively, which is characteristic of the Bi^{3+} in bismuth oxyhalides. In the Fig. 4c the O1s spectrum was shown which can be fitted into two peaks. The main peak at 526.7 eV was attributed to the Bi-O bond in $[Bi_2O_2]^{2+}$ slabs of BiOClBr IL structure.

The other peak at 530.9 eV is mainly attributed to H_2O or OH^- adsorbed at the surface. The peaks with binding energies of 197.4 eV and 199.9 eV (Figure 4d) were referred to the Cl $2p_{3/2}$, Cl $2p_{1/2}$ and confirmed monovalent chlorine state. The Br 3d XPS spectra presented in Figure 4e exhibit two main peaks with BE 68.1 eV and 69.9 eV, corresponding to Br $3d_{5/2}$ and Br $3d_{3/2}$, respectively.

Both halogens peaks were assigned at monovalent oxidation state. The results for BiOCl, BiOBr and BiOClBr were similar.

The XRD and XPS results confirmed that the BiOClBr IL sample is solid solutions and imidazolium ionic liquids used as a halides sources were removed from the surface of BiOClBr IL.

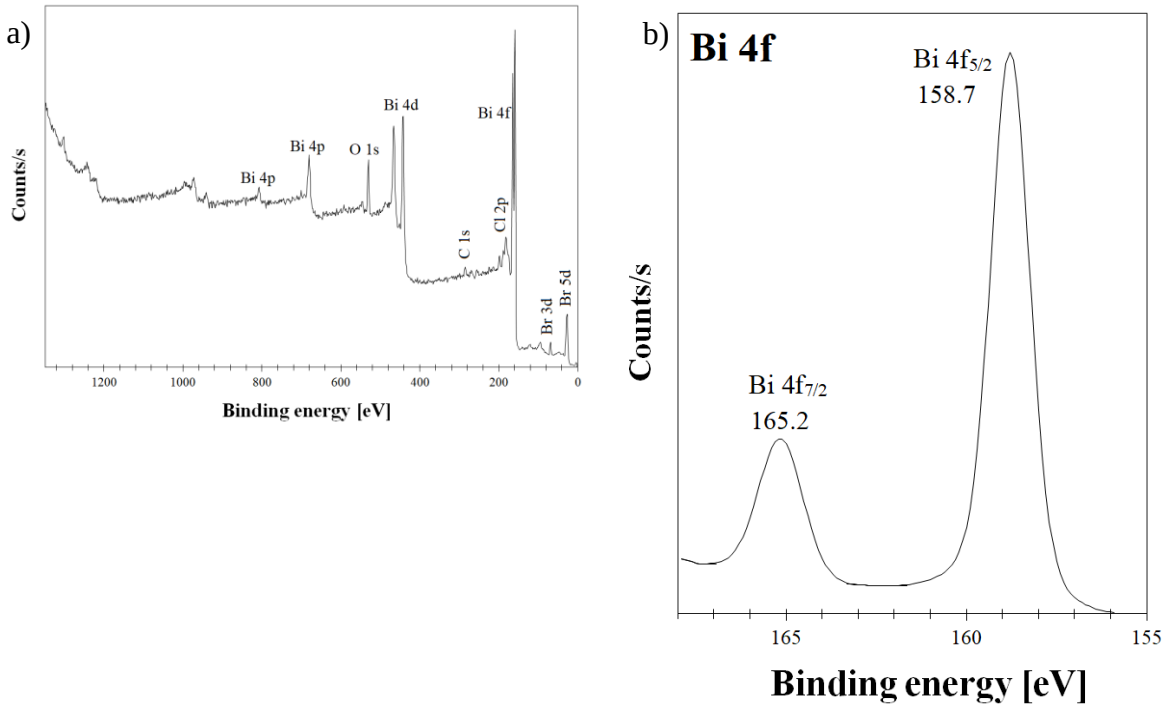

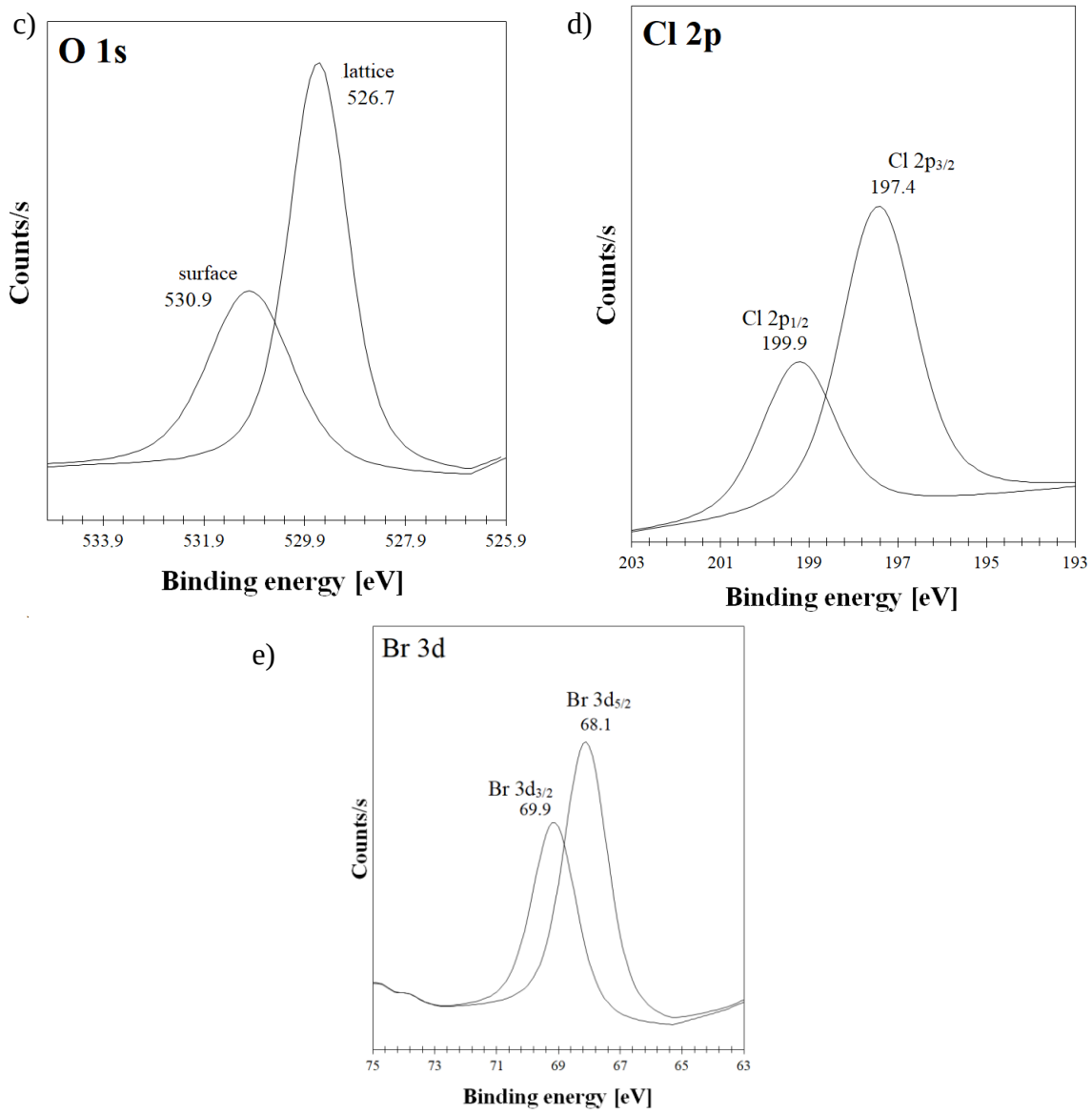

Fig 4. High resolution spectra XPS of BiOClBr IL: a) Total survey, b) Bi 4f, c) O 1s, d) Cl 2p and e) Br 3d.

3.7. *Effect of pH on photocatalyst surface*

The pH_{zpc} value is an important property of the photocatalysts and relating to the phenomenon of adsorption of the pollutants. The pH_{zpc} was examined for BiOCl IL and BiOClBr IL and its value was 5.78 and 5.58, respectively (Fig S1). At a pH below pH_{zpc} the photocatalyst surface is positively charged, while it is negatively charged above pH_{zpc}. The pH value of photocatalyst mixed with 5-fluorouracil, cyclophosphamide and imatinib during photodegradation

experiments varied from 5.26 to 4.86. This indicated that the surface was positively charged throughout the irradiation.

Additionally, 5-FU (pKa_1=7.5; pKa_2=9.0) and CP (pKa= pKa_1=2.3 pKa_2=11.1) in mixture existed mainly in the neutral form, while IMA was the cation protonated at nitrogen in piperazine ring located at the end of the large molecule of studied drug. The localization of positive electric charge did not affect the IMA adsorption on the photocatalysts surface.

3.8. *Photocatalytic activity*

The photocatalytic activity of fabricated photocatalysts in degradation of three cytostatic drugs: 5-FU, CP and IMA was investigated. Due to the similar crystal phase, the effects of BiOCl and BiOClBr on cytostatic drugs removal under UV-Vis light irradiation were compared. Photolysis of used model micropollutants in experimental pH were negligible . The kinetics data of drugs photodegradation correlated well with the pseudo-first order model (Table 4).

In the Fig 5 the variations of concentration of 5-FU (a), CP (b) and IMA (c) in the function irradiation time in the presence of 0.5 g L^{-1} photocatalyst: BiOCl, BiOCl IL, BiOClBr and BiOClBr IL were shown. In case of 5-FU drug adsorption at the surface of the all studied photocatalysts was very low and independent of the preparation procedure. After 90 min of irradiation, 5-FU was totally degraded over BiOCl, while the process lasted 120 min for BiOCl IL. In the case of BiOClBr 5-FU the removal was complete after 90 and 120 min for sample fabricated with ILs and KCl/KBr respectively. BmimX used as a halogen source in the photocatalyst preparation resulted in a 2 times decreased of BiOCl IL activity in drug degradation process compared to BiOCl, while the activity of BiOClBr IL increased 1.4 times for BiOClBr. This indicated that ILs improved the photocatalytic activity of samples BiOClBr IL prepared by the solvothermal method, while the results for BiOCl are challenging to interpret

due to the 1.6 higher surface area with active centers of the BiOCl compared to the surface of BiOCl IL.

Table 2. Comparison of the photocatalytic performance of BiOX with reaction rate constants (k) for model micropollutants under artificial solar light.

Photocatalyst	5-FU		CP		IMA	
	k min^{-1}	R^2	k min^{-1}	R^2	k min^{-1}	R^2
BiOCl	0.0361	0.9917	0.0011	0.9966	0.0313	0.9942
BiOCl IL	0.0247	0.9938	0.0011	0.9966	0.0403	0.9962
BiOClBr	0.0216	0.9925	0.0075	0.9992	0.0479	0.9954
BiOClBr IL	**0.0569**	0.9935	**0.0164**	0.9918	**0.0486**	0.9994

The adsorption of CP on the surface of all samples was negligible. The rate of CP decomposition was higher over BiOClBr than BiOCl, independently of the sample preparation method. After 120 min of irradiation 79% and 58% of CP was degraded under BiOClBr IL and BiOClBr, respectively. ILs used for the preparation of photocatalyst improved BiOClBr activity towards CP. CP removal under BiOCl and BiOCl IL was lower when compared to BiOClBr and reached in the same time only 12%. Photocatalytic decomposition rate of CP was not elevated by the IL applied to BiOCl fabrication, while this rate was 2.2 times faster for BiOClBr prepared with the IL. The results also indicated that under experimental conditions CP is a more resistant compound than 5-FU in photocatalysis under BiOClBr IL.

IMA was adsorbed at all samples with the increase trend in the following order BiOCl ≈ BiOCl IL < BiOClBr IL < BiOClBr. It was observed (Fig 5c), that after 120 min of UV-Vis light irradiation IMA was completely removed by using the all of studied photocatalysts. Furthermore, the apparent rate constants *k* of BiOClBr IL and BiOClBr was significantly higher than that of the single halogen BiOCl sample.

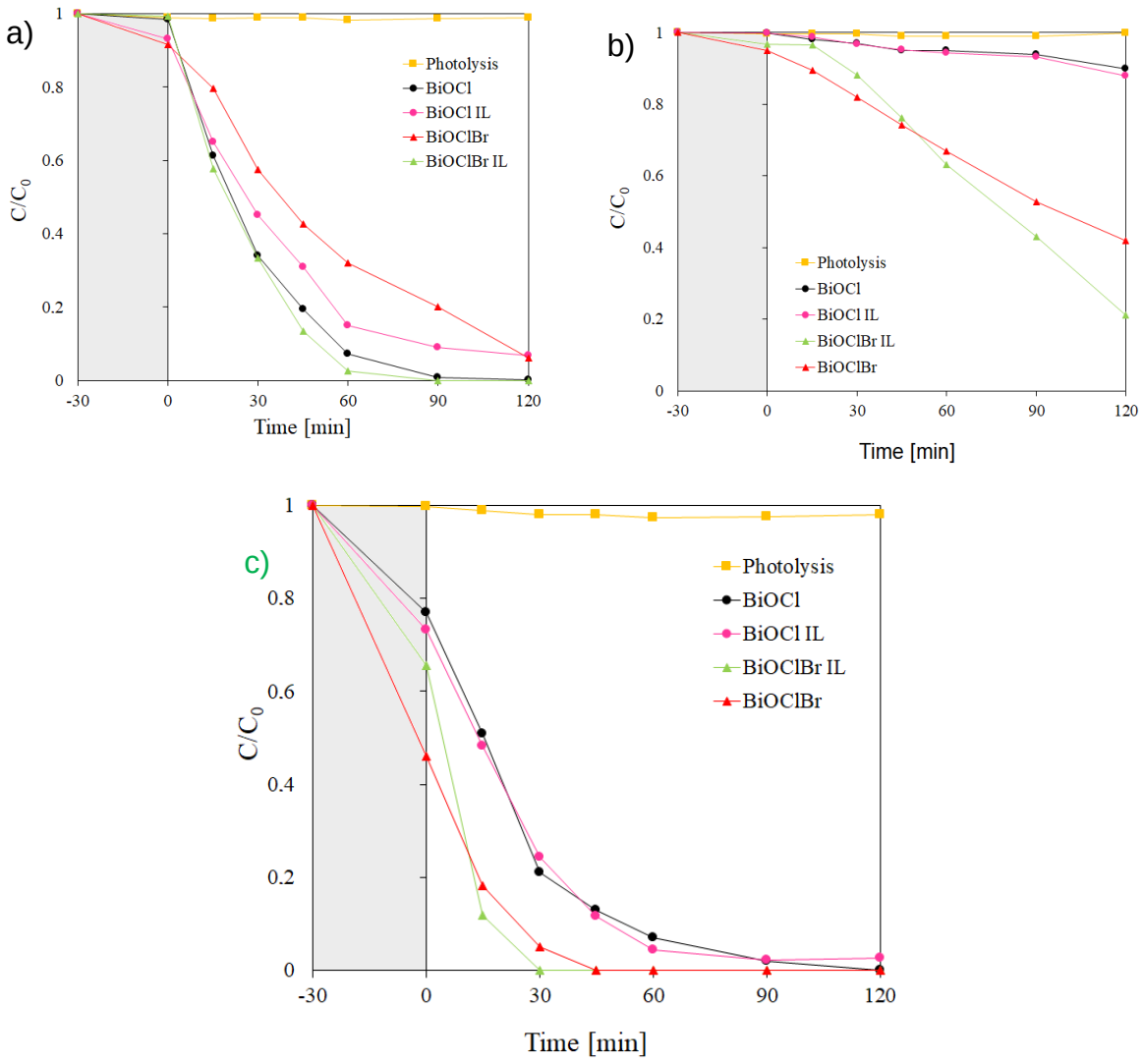

Fig. 5 Photocatalysis decomposition a) 5-fluorourail, b) cyclophosphamide, c) imatinib in presence of prepared photocatalysts under solar light irradiation.

The results clearly indicated that the BiOClBr IL prepared using BmimCl and BmimBr as the source of halogens demonstrated the best activity toward all studied cytostatic drugs degradation under UV-Vis light. They resistivity in photocatalytic process was in the following order CP > 5-FU > IMA. BiOCl and BiOCl IL samples demonstrated the similar activity

towards CP and IMA degradation or lower activity of BiOCl IL than BiOCl for 5-FU oxidation. The fact suggested that the mechanism of studied drugs degradation was different.

3.9. *TOC and TN removal*

The ability of photocatalysts to mineralized 5-FU, CP and IMA were evaluated by variation in concentration of TOC and TN after 2h of irradiation. The results presented in Table 3 indicated that BiOClBr prepared with or without ILs used, characterized better photocatalytic activity in mineralization of drugs than BiOCl and BiOCl IL with single halide. Both BiOClBr and BiOClBr IL removed TOC and TN, however the mineralization was more advanced under sample prepared with the ILs. In the presence of BiOClBr IL the mineralization reached 24.5, 15.6 and 39.3% of TOC removal for 5-FU, CP and IMA, respectively. The production of gaseous nitrogen was higher under BiOClBr for 5-FU (9.4%) and CP (13.9%) than BiOClBr IL, while for IMA the situation was different and in the presence of BiOClBr IL TN (16.4%) was removed at a higher efficiency than in the presence of BiOClBr (13.6%). Obtained nitrogen removal by BiOClBr was probably synergistic effect of metallic Bi, $Bi_4O_5Br_2$ and BiOCl phase presence in the photocatalyst. In 5-FU and CP solution, the equilibrium between TOC and TN removal under BiOClBr IL was shifted towards the removal of TOC, while under BiOClBr towards TN removal. The mechanism of IMA mineralization was different, and TOC and TN removal increased under BiOClBr IL compare to the mineralization of the drug under BiOClBr. The results indicated that the synthesis BiOClBr IL via ILs produced a photocatalysts with a higher ability to mineralize the micropollutants and to remove the nitrogen as a N gaseous products form water, which is very beneficial for the environmental applications.

Table 3. Total organic carbon and total nitrogen removal [%].

Photocatalyst	5-FU		CP		IMA	
	TOC_{rem}	**TN_{rem}**	**TOC_{rem}**	**TN_{rem}**	**TOC_{rem}**	**TN_{rem}**
BiOCl	2.3	0	0	0	28.5	7.0
BiOCl IL	10.1	0	0	0	29.2	6.6
BiOClBr	19.8	**9.4**	0	**13.9**	33.1	13.6
BiOClBr IL	**24.8**	5.0	15.6	2.9	**39.3**	**16.4**

rem - removal

3.10. *Mechanism of photocatalytic decomposition of studied drugs*

The mechanisms of cytostatic drugs degradation were studied under the BiOClBr IL with the highest photocatalytic activity. In the Fig. 6a were shown the results of photocatalytic decomposition of 5-FU, CP and IMA in the presence of Na_2EDTA, t-butyl alcohol, ascorbic acid and chloroform used as a holes, $^{\bullet}OH$, $^{\bullet}O_2^{-}$ and e^- scavengers, respectively. The degradation of 5-FU was significantly decelerated in presence the of Na_2EDTA, while the addition of ascorbic acid inhibited this process in 44%. *Tert*-butyl alcohol and chloroform influence was negligible the process. The result suggested that 5-FU using BiOClBr IL was decomposed mainly by h^+ and next by $^{\bullet}O_2^-$. The experiments with photocatalytic oxidation of terephalic acid and NBT (Fig. S2) confirmed the lack of $^{\bullet}OH$ radicals generation and presence of $^{\bullet}O_2^-$ in system with BiOClBr IL. The finding was agreement with the literature reports, suggesting that photocatalyst BiOX generated h^+ and $^{\bullet}O_2^-$ [21].

CP decomposition performed in the presence of selected scavengers showed that $^{\bullet}O_2^-$, h^+, and e^- were participated in the degradation of CP under BiOClBr IL. The $^{\bullet}O_2^-$ was capable of reacting with a variety of substrates owing to its anionic, radical, and redox nature, although the nucleophilic and reducing electron transfer processes appear to be the predominate reaction pathways [48]. Due to CP is a chloroorganic oxyphosphorous derivative (Table 1) the nucleophilic reaction with $^{\bullet}O_2^-$ is possible as well as the reduction by electrons [49-50] as presented below:

$RCH_2Cl + {}^{\bullet}O_2^- \rightarrow RCH_2OO^{\bullet} + Cl^-$ (1)

$RCH_2Cl + 2e^- + H^+ \rightarrow RCH_3 + Cl^-$ (2)

These products, could be produced by the electron reduction as was reported in literature [51]. The CP byproduct with $[M+H]^+ = 227$ in the effluents after UV/TiO_2 treatment and its structure suggested that CP was transformed by the electron-reduction process. In our study the presence of $[M+H]^+ = 227$ in the mixture after photocatalysis using BiOClBr IL was also confirmed by LC-MS.

IMA decomposition was intensively inhibited primarily by L-ascorbic acid ($^{\bullet}O_2^-$ scavenger) and in secondly by Na_2EDTA (h^+). There were no verity in removal efficiency of the micropollutant in the presence of *tert*-butyl alcohol and chloroform into the system.

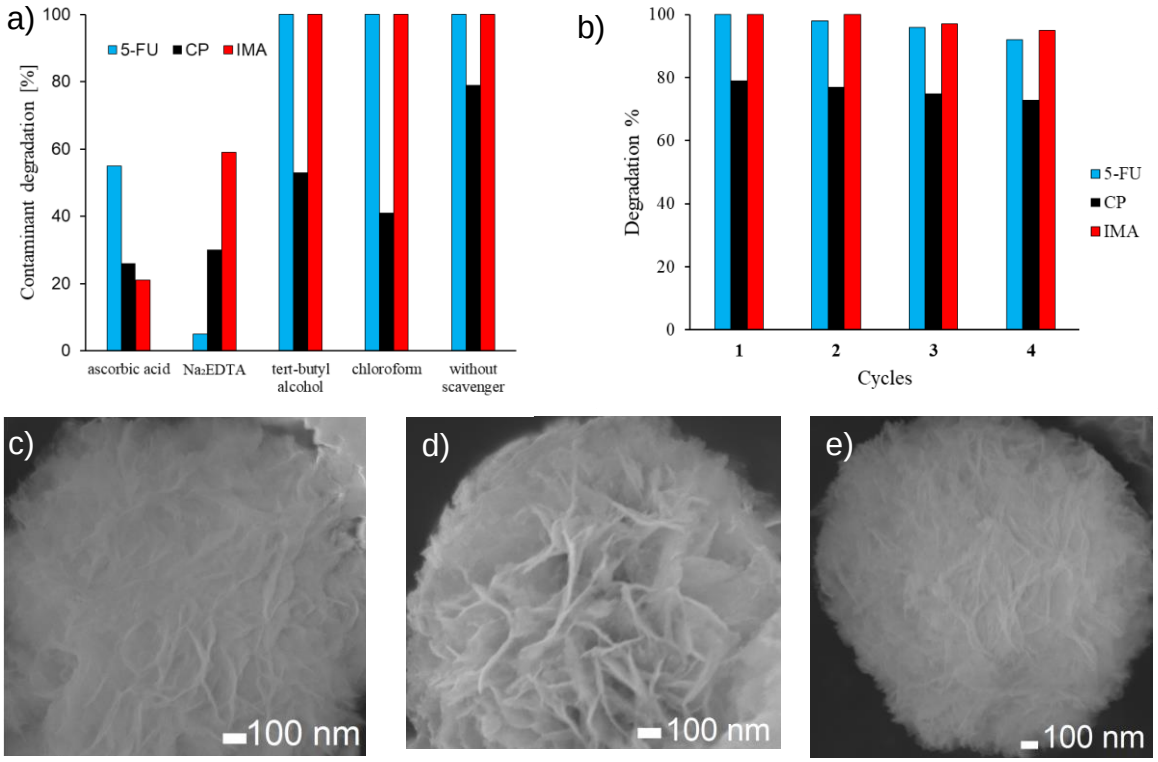

Fig. 6. a) Effects of reactive species on photocatalytic degradation of 5-fluorouracil, cyclophosphamide and imatinib over BiOClBr IL; b) Stability study for photodegradation of 5-FU, CP and IMA and SEM pictures after decomposition of c) 5-FU, d) CP and e) IMA over BiOClBr IL.

The results indicated that studied cytostatic drugs were degraded under BiOClBr IL by different mechanisms. The 5-FU was the most reactive with photogenerated h^+, while IMA was mainly degraded by $^{\bullet}O_2^-$. In CP removal h^+ and $^{\bullet}O_2^-$ participated with the similar extent, but in contrast to 5-FU and IMA, the electron reduction of CP was also possible.

The differences between the TOC and TN removal during 5-FU and IMA oxidation can be explained by the fact, that h^+ mainly participated in the organic matter oxidation, while $^{\bullet}O_2^-$ can react with nitrogen located in the aromatic rings of IMA and likely oxidized it to N gaseous products.

3.11. *Stability of BiOClBr IL*

The stability and reusability of the BiOClBr IL for photocatalytic degradation of 5-FU, CP and IMA were examined. The photocatalyst were reused four times for the photocatalysis under the same reaction conditions. The results are shown in Fig. 6b. The degradation efficiency of BiOClBr IL decreased by 9, 6 and 5% for 5-FU, CP and IMA respectively. Furthermore, SEM images revealed that nanoparticles of BiOClBr IL maintained the structure of the flower-like microspheres and the damages of nanosheets were almost invisible after 4 cycles (Fig. 6 cde). These observations suggest that BiOClBr IL has good photostability.

4. Conclusions

In this work, a series of BiOCl, BiOBr and BiOClBr were synthesized using a two steps solvothermal reaction in glycerol where inorganic salts (KCl, KBr) or ILs (BmimCl, BmimBr) were used as a source of halides. All samples, except BiOBr, were assembled into regular flower-like microspheres while BiOBr was the hierarchical material without distinguished

individual nanosheets. A possible formation mechanism of the flowerlike microspheres is proposed and illustrated at Fig. 7.

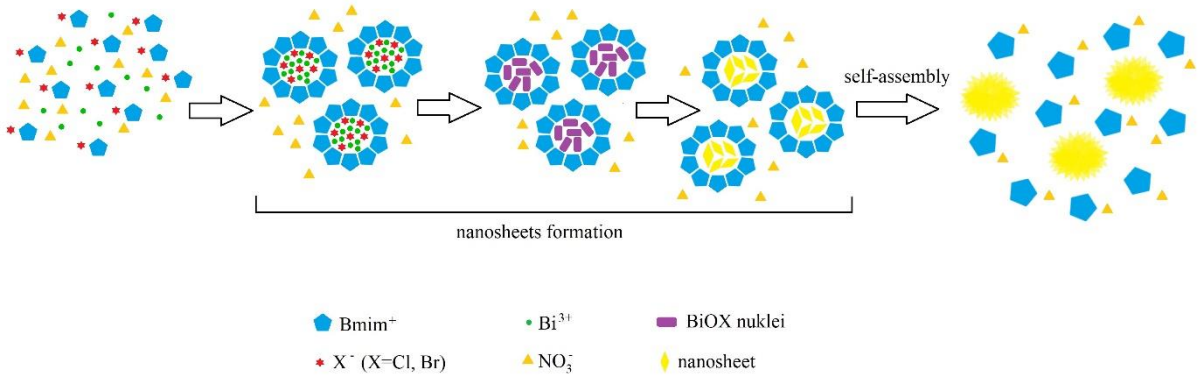

Fig. 7. Schematic illustration of proposed formation mechanism of BiOX flowerlike microstructures.

At the beginning the reactants were ordered into micelles as a consequence of the ionic liquid based on imidazolium cations aggregations behavior into micelles in the solutions. The reaction between ordered reactants formed BiOX nuclei in the micelle centre. These nuclei gradually grew into nanosheets embedded in the micelles to form aggregates and then self-assembled into flowerlike microspheres. Close nearness of imidazolium cations and, consequently, chemical interactions between the obtained nanosheets and $Bmim^+$, bends nanosheets. The flowerlike BiOX microspheres were obtained after washing out the Bmim cations. In this process, BmimX functioned as an halogen source and template and solvent and was essential for the structure of BiOBr and BiOClBr. Further work is still needed to investigate the exact growth mechanism. The proposed method of the synthesis allowed to obtain BiOCl phase, BiOClBr solid solution and $Bi_4O_5Br_2$ phase. The XPS and FT-IR analysis confirmed the complete removal of BmimX ILs form surface of the photocatalysts. Bismuth-based photocatalyst BiOClBr prepared via ILs was more efficient for degradation of studied cytostatic drugs under UV-Vis irradiation. The BiOClBr IL sample was also characterized the highest drugs mineralization, while BiOClBr

was more effective in N gaseous products production. The efficiency and rate of drugs removal increased in the following order: CP < 5-FU < IMA. The drug's degradation mechanism in the presence of BiOClBr IL was also evaluated. Their degradation mechanism was different: 5-FU was mainly oxidized by h^+, IMA by $^{\bullet}O_2^-$, while CP was degraded by h+ and $^{\bullet}O_2^-$ and photogenerated e^- could also participate in this process. Our findings are very promising for the applications of the bismuth based photocatalysts in the water treatment and grant a new perspective on the cytostatic drugs degradation mechanism.

Acknowledgment

The Authors would like to thank dr hab. Anna Zielińska-Jurek of The Department of Chemical Technology, Faculty of Chemistry, Gdansk University of Technology for allowing the use of this Surface Area and Pore Size Analyzer and dr Anna Malankowska of Faculty of Chemistry of the University of Gdansk for the SEM images. The authors would like to acknowledge the financial support of the Polish Ministry of Science and Higher Education under the grant DS 530-8626-D596-18, BMN 538-8626 B806-18 and National Science Center within program MINIATURA 1 grant DEC-2017/01X/ST5/01136.

REFERENCES

[1] J. Rivera-Utrilla, M. Sanchez-Polo, M.A Ferro-Garcia, G. Prados-Joya, R. Ocampo-Perez, Pharmaceuticals as emerging contaminants and their removal form water, Chemosphere 93 (2013) 1268-1287.

[2] J.F. Zhang, V.W.C. Chang, A. Giannis, J.Y. Wang Removal of cytostatic drugs from aquatic environment: a review**,** Science of the Total Environment 445–446 (2013) 281-298.

[3] T. Kosjek, T. Heath, Occurrence, fate and determination of cytostatic pharmaceuticals in the environment, TrAC Trends in Analytical Chemistry 30 (2011) 1065 – 1087.

[4] H. Franquet-Griell, A. Medina, C. Sans, S. Lacorte, Biological and photochemical degradation of cytostatic drugs under laboratory conditions, Journal of Hazardous Materials 323 (2017) 319-328.

[5] C. Ort, M.G. Lawrence, J. Reungoat, G. Eaglesham, S. Carter, J. Keller, Determining the fraction of pharmaceutical residues in wastewater originating from a hospital**,** Water Research 44 (2010) 605-615.

[6] K. Kummerer, Antibiotics in the aquatic environment – a review. Part I, Chemosphere 75 (2009) 417-434.

[7] D. Zhang, R.M Gersberg, W.J. Ng, S.K. Tan, Removal of pharmaceuticals and personal care products in aquatic plant-based systems: A review, Environmental Pollution 184 (2014) 620-639.

[8] B.G. Zheng, Z. Zheng, J.B. Zhang, X.Z Luo, J.Q Wang, Q. Liu, L.H. Wang, Degradation of the emerging contaminant ibuprofen in aqueous solution by gamma irradiation, Desalination 276 (2011) 379-385.

[9] O. Frederic, P. Yves, Pharmaceuticals in hospital wastewater: their ecotoxicity and contribution to the environmental hazard of the effluent, Chemosphere 115 (2014) 31-39.

[10] J.C. Madden, S.J. Enoch, M. Hewitt, M.T.D. Cronin, Pharmaceuticals in the environment: Good practice in prediction their ecotoxicological effects, Toxicology Letters 185 (2009) 85-101.

[11] J. Li, Y. Yu, L. Zhang, Bismuth oxyhalides nanomaterials: layer structures meet photocatalysis, Nanoscale 6 (2014) 8473-8486

[12] Z-c. Zhu, P. Chen, X-h, R-x. Wang, BiOBr three-dimensional micromaterials in a solvothermal system and their photocatalytical property under visible-light irradiation, Journal of Experimental Nanoscience 10 (2015) 564-575.

[13] H. Deng, J. Wang, Q. Pemg, X. Wang, Y. Li, Controlled Hydrothermal synthesis of Bismuth Oxyhalide Nanobelts and Nanotubes, Chemistry – A European Journal 11 (2005) 6519-6524.

[14] J. Zhang, J. Xia, S. Yin, H. Li, H. Xu, M. He, L. Huang, Improvement of visible light photocatalytic activity over flower-like BiOCl/BiOBr microspheres synthesized by redactable ionic liquids, Colloids and Surfaces A: Physiochemical and Engineering Aspects 420 (2013) 89-95.

[15] Q. Hu, M. Ji, J. Di, B. Wamg, J. Xia, Y. Zhao, H. Li, Ionic-liquid-induced double regulation of carbon quantum dots modified bismuth oxychloride/bismuth oxybromide nanosheets with enhanced visible-light photocatalytic activity, Journal of Colloid and Interface Science 519 (2018) 263-272.

[16] J. Yang, Y. Liang, K. Li, Y. Zhu, S. Liu, R. Xu, W. Zhou, Design of 3D flowerlike BiOClxBr1-x nanostructure with high surface area for visible light photocatalytic activities, Journal of Alloys and Compounds 725 (2017) 1144-1157.

[17] D. Zhang, G. Li, X. Yang, J.C. Yu, A micrometer-size TiO_2 single-crystal photocatalyst with remarkable 80% level of reactive facets, Chemical Communications 29 (2009) 4381-4383.

[18] J. Xia, S. Yin, H. Li, H. Xu, Y. Yan, Q. Zhang, Self-assembly and enhance photocatalytic properties of microspheres via reactable ionic liquid, Langmuir 27 (2011) 1200-1206.

[19] J. Xia, J. Zhang, S. Yin, H. Li, X. Xu, L. Xu, Q. Zhang, Advanced visible light photocatalytic properties of BiOCl micro/nanospheres synthesized via reactable ionic liquids, Journal of Physics and Chemistry of Solids 74 (2013) 298-304.

[20] P. Wang, P. Yang, B. Yang, T. Chen, X. Shi, L. Ye, X. Zhang, Synthesis of 3D BiOBr microspheres for enhanced photocatalytic CO_2 reduction, Journal of the Taiwan Institute of Chemical Engineers 68 (2016) 295-300.

[21] J. Xia, Y. Ge, J. Di, L. Xu, S. Yin, Z. Chen, P. Liu, H. Li, Ionic Liquid-Assisted Strategy for Bismuth-Rich Bismuth Oxybromides Nanosheets with Superior Visible Light-Driven Photocatalytic Removal of Bisphenol A, Journal of Colloid and Interface Science 473 (2016) 112-119.

[22] J. Zhang, J. Xia, S. Yin, H. Li, H. Xu, M. He, L. Huang, Q. Zhang, Improvement of visible light photocatalytic activity over flower-like BiOCl/BiOBr microspheres synthesized by reactable ionic liquids, Colloids and Surfaces A: Physiochemical and Engineering Aspects 420 (2013) 89-95.

[23] Q. Qin, Y. Guob, D. Zhoua, Y. Yanga, Y. Guoa, Facile growth and composition-dependent photocatalytic activity of flowerlike $BiOCl1_{-x}Br_x$ hierarchical microspheres, Applied Surface Science 390 (2016) 765–777

[24]-X. Qin, H. Cheng, W. Wang, B. Huang, X. Zhang, Y. Dai, Three dimensional BiOX (X=Cl, Br and I) hierarchical architectures: facile ionic liquid-assisted solvothermal synthesis and photocatalysis towards organic dye degradation, Materials Letters 100 (2013) 285-288.

[25] Y. Bai, L. Ye, T. Chen, P. Wang, L. Wang, and X. Shi, Synthesis of hierarchical bismuth-rich $Bi_4O_5B_{rx}I_{2-x}$ solid solutions for enhanced photocatalytic activities of CO 2 conversion and Cr (VI) reduction under visible light, Applied Catalysis B: Environmental. 203 (2017) 633–640.

[26] S. Yadav, V. Srivastava, S. Banerjee, C-H. Weng, Y.C. Sharma, Adsortion characteristics of modified sand for the removal of hexavalent chromium ions from aqueous solutions: Kinetic, thermodynamic and equilibrium studies, CATENA 100 (2013) 120-127.

[27] K. Mioduszewska, J. Dolzonek, D. Wyrzykowski, L. Kubik, P. Wiczling, C. Sikorska, M. Tonski, Z. Kaczynski, P. Stepnowski, A. Bialk-Bielinska, Overview of experimental and computational methods for the determination of the pKa values of 5-fluorouracil,

cyclophosphamide, ifofamide, imatinib, methotrexate, Trends in Analytical Chemistry 97 (2017) 283-296.

[28] M. Tonski, J. Dolzonek, M. Paszkiewicz, J. Wojslawski, P. Stepnowski, A. Bialk-Bielinska, Preliminary evaluation of the application of carbon nanotubes as a potential adsorbents for the elimination of selected anticancer drugs from water matrices, Chemosphere 201 (2018) 32-40.

[29] D. Sun, J. Li, Z. Femg, L. He, B. Zhao, T. Wang, R. Li, S. Yin, T. Sato, Solvothermal synthesis of BiOCl flower-like hierarchical structures with high photocatalytic activity, Catalysis Communications 51 (2014) 1-4.

[30] H-Y. Hao, Y-Y.Xu, P. Liu, G-Y. Zhang, BiOCl nanostructure with different morphologies: Tunable synthesis and visible-light-driven photocatalytic properties, Chinese Chemical Letters 26 (2015) 133-136.

[31] S. Yin, J. Di, M. Li, W. Fan, J. Xia, H. Xu, Y. Sun, H. Li, Synthesis of Multiwalled Carbon Nanotube Modified BiOCl Microspheres with Enhanced Visible-Light Response Photoactivity, CLEAN Soil Air Water 44 (2016) 781–787.

[32] M. Li, Y. Cui, Y. Jin, H. Li, Facile hydrolysis synthesis of $Bi_4O_5Br_2$ photocatalyst with excellent visible light photocatalytic performance for the degradation of resorcinol, RSC Advances 6 (2016) 47486-47490.

[33] J. Xia, Y. Ge, J. Di, L. Xu, Z. Chen, P. Liu, H. Li, Ionic liquid-assisted strategy for bismuth-rich bismuth oxybromides nanosheets with superior visible light-driven photocatalytic removal of bisphenol-A, Journal of Colloid and Interface Science 473 (2016) 112-119.

[34] L. Leonite, M. Caraman, M. Alexe, C. Harnagea, Structural and optical characteristics of bismuth oxide thin films, Surface Science 507-510 (2002) 480-485.

[35] Z. Chen, J. Zeng, J. Di, D. Zhao, M. Ji, J. Xia, H. Li, Facile microwave-assisted ionic liquid synthesis of sphere-like BiOBr hollow and porous nanostructures with enhanced photocatalytic performance, Green Energy & Environment 2 (2017) 124-133.

[36] C. Liu, X. Dong, Y. Hao, X. Wang, H. Ma, X. Zhang, Efficient photocatalytic dye degradation over Er-doped BiOBr hollow microspheres wrapped with graphene nanosheets: enhanced solar energy harvesting and charge separation, RSC Advances 36 (2017) 22415-22423.

[37] J. Zhang, J. Lv, K. Dai, C. Liang, Q. Liu, One-step growth of nanosheet-assembled BiOCl/BiOBr microspheres for highly efficient visible photocatalytic performance, Applied Surface Science 430 (2018) 639-646.

[38] W. Wang, F. Haung, X. Lin, J. Yang, Visible-light-responsive photocatalysts xBiOBr-(1-x)BiOI, Catalysis Communications 9 (2008) 8-12.

[39] R. Zhao, X. Li, Y. Zhai, Q. Li, Effect of Chlorine Source on the Morphology of Flower-like BiOCl and its Photocatalytic Activity, Journal of Advanced Oxidation Technologies 18 (2015) 353-360.

[40] T. B. Li, G. Chen, C. Zhou, Z.Y. Shen, R.C Jin, J.X Sun, New Photocatalyst BiOCl/BiOI Composites with Highly Enhanced Visible Light Photocatalytic Performances, Dalton Transactions 40 (2011) 6751-6758.

[41] X. Xiao, M. Lu, J. Nan, X. Zuo, W. Zhang, S. Liu, S. Wang, Rapid microwave synthesis of I-doped $Bi_4O_5Br_2$ with significantly enhanced visible-light photocatalysis for degradation of multiple parabens, Applied Catalysis B: Environmental 218 (2017) 398-408.

[42] W. Zhang, X. Liu, F. Dong, Y. Zhang, Facile synthesis of $Bi_{12}O_{17}Br_2$ and $Bi_4O_5Br_2$ nanosheets: O=In situ DRIFTS investigation of photocatalytic NO oxidation conversion pathway, Chinese Journal of Catalysis 38 (2017) 2030-2038.

[43] X. Zhang, L-W. Wang, C-Y. Wang, W-K. Wang, Y-L. Chen, Y-X. Haung, W-W. Li, Y-J. Feng, H-Q. Yu, Synthesis of BiOClxBr1-x Nanoplate Solid Solutions as a Robust Photocatalyst with Tunable Band Structure, Chemistry – a European Journal 21 (2015) 11872-11877.

[44] Y. Liu, W-J Son, J. Lu, B. Huang, Y. Dai, M-H. Whangbo, Composition Dependence of the Photocatalytic Activities of BiOCl1-xBrx Solid State Solution under Visible Light, Chemistry – A European Journal 17 (2011) 9342-9349.

[45] H. Gnayem, Y. Sasson, Semiconductors with Expectational Visible Light Photocatalytic Activity, ACS Catalysis 3 (2013) 186-191.

[46] B. Zhang, G. Ji, Y. Liu, M.A. Gondal, X. Chang, Efficient adsorption and photocatalytic performance of flower-like three dimensional (3D) I-doped BiOClBr photocatalysts, Catalysis Communications 36 (2013) 25-30.

[47] D. Yang, M.A. Gondal, Z.H, Yamani, Q. Xu, D. Xiang, M. Junkui, K. Shen, Enhanced Photosensitization Decomposition of Rhodamine B onto BiOCl Nanosheets with Controllable-Exposed {001} Facets, Nanoscience and Nanotechnology Letters 11 (2016) 938-945.

[48] W.C Danen, R.J. Warner, R.L Arudi, Nucleophilic Reactions of Superoxide Anion Radical, Organic Free Radicals 14 (1978) 244-257.

[49] S. Susarla, S. Masunaga, Y. Yonezewa, Reductive pathways of chloroorganics under anaerobic conditions, Water Science and Technology 34 (1996) 489-494.

[50] Y. Yasman, V. Bulatov, I. Rabin, M. Binetti, I. Schechter, Enhanced electro-catalytic degradation of chloroorganic compounds in the presence of ultrasound, Ultrasonics Sonochemistry 13 (2006) 271-277.

[51] W.W. Lai, H. H. Lin, A. Y. Lin, TiO_2 photocatalytic degradation and transformation of oxazaphosphorine drugs in an aqueous environment, Journal of Hazardous Materials 287 (2015) 133–141.

[52] K. Vanheusden, C.H. Seager, W.L. Warren, D.R. Tallant, J. A. Voigt, Correlation between photoluminescence and oxygen vacancy in ZnO phosphors, Applied Physics Letters 68 (1996) 403-407.

SUPPLEMENTARY DATA

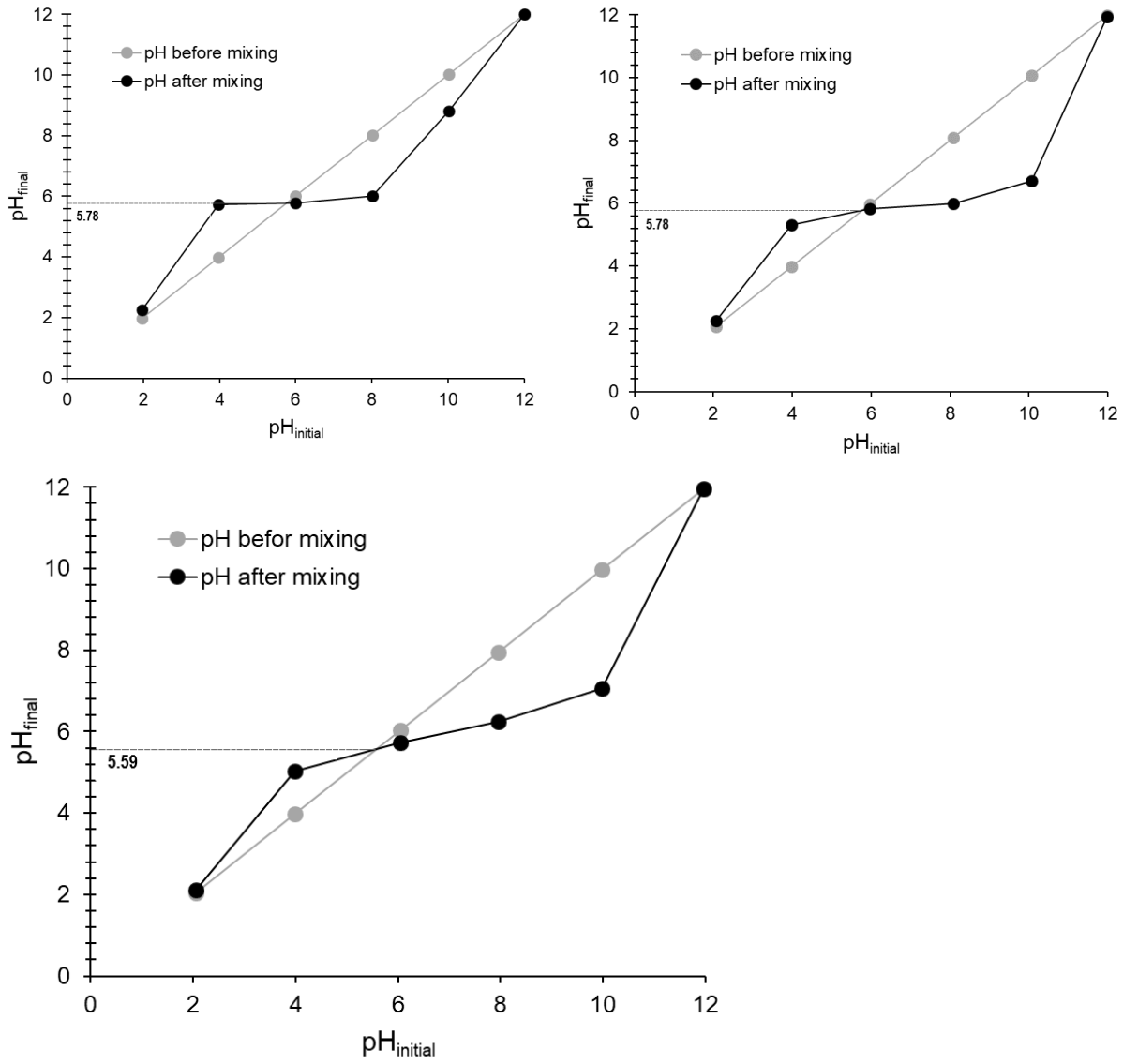

Fig S1. pH_{zpc} of a) BiOCl b) BiOCl IL and c) BiOClBr IL

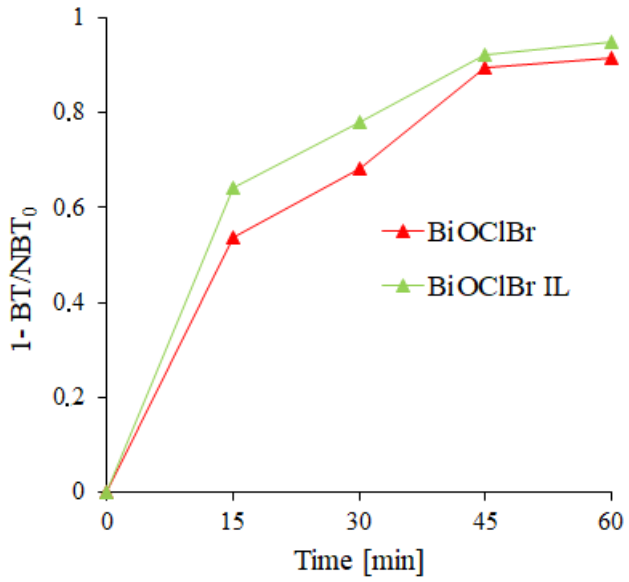

Fig S2. Photocatalytic reaction of NBT.

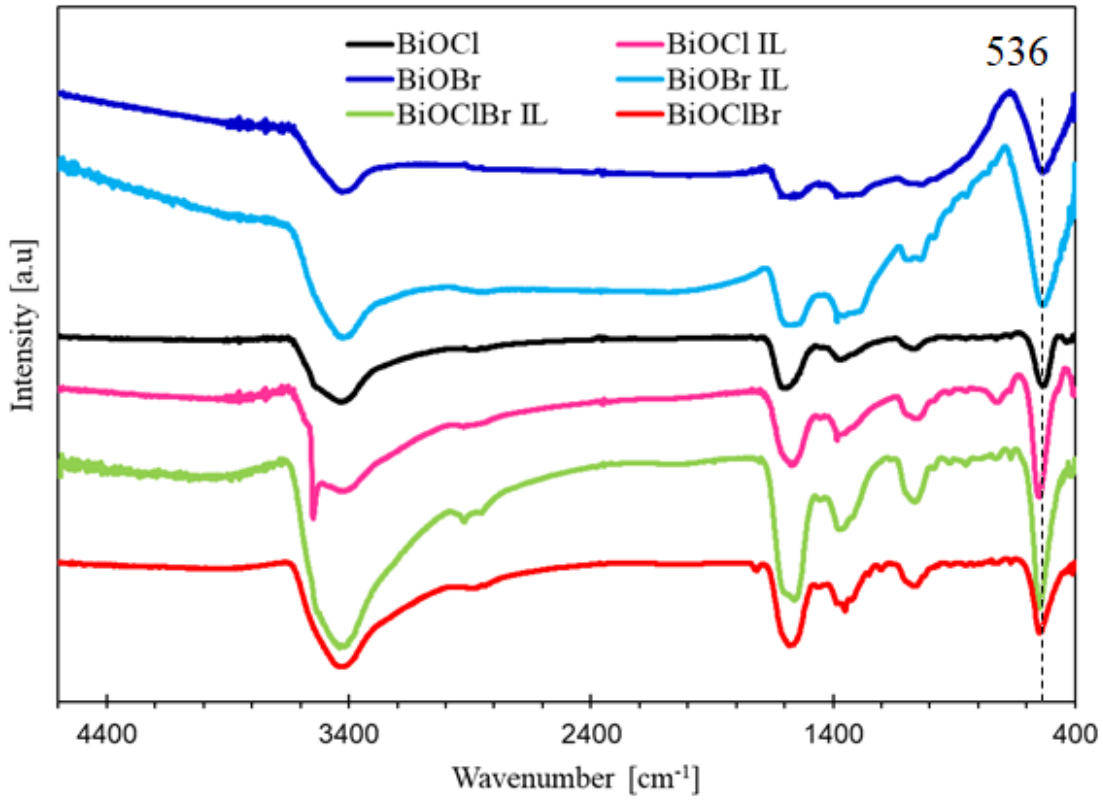

Fig S3. Differences FT-IR spectra of as-prepared photocatalysts.

PL spectra analysis

To investigate the effect of ionic liquid used in synthesis on the separation and generation efficiency of photogenerated electrons and holes and in consequence photocatalytic activity BiOX and BiOXY samples were characterized by means of PL spectra and results are shown in Fig. 4. As shown Fig. S4 PL intensity difference between BiOCl and BiOCl IL was not observed. PL intensity of BiOBr was significantly lower than BiOBr IL. According to XRD analysis BiOBr samples containing mostly $Bi_2O_5Br_2$ which has more oxygen vacancy than BiOBr. It was observed by Vanheusden group [52] that stronger PL intensity can comes from a higher concentration of oxygen vacancy and owing to this more efficient photocatalytic activity could be achieved. The shape of BiOClBr and BiOClBr IL spectra showed higher similarities to BiOCl than BiOBr. BiOClBr showed lower peak intensity than BiOClBr IL suggesting that has more oxygen vacancy than BiOClBr.

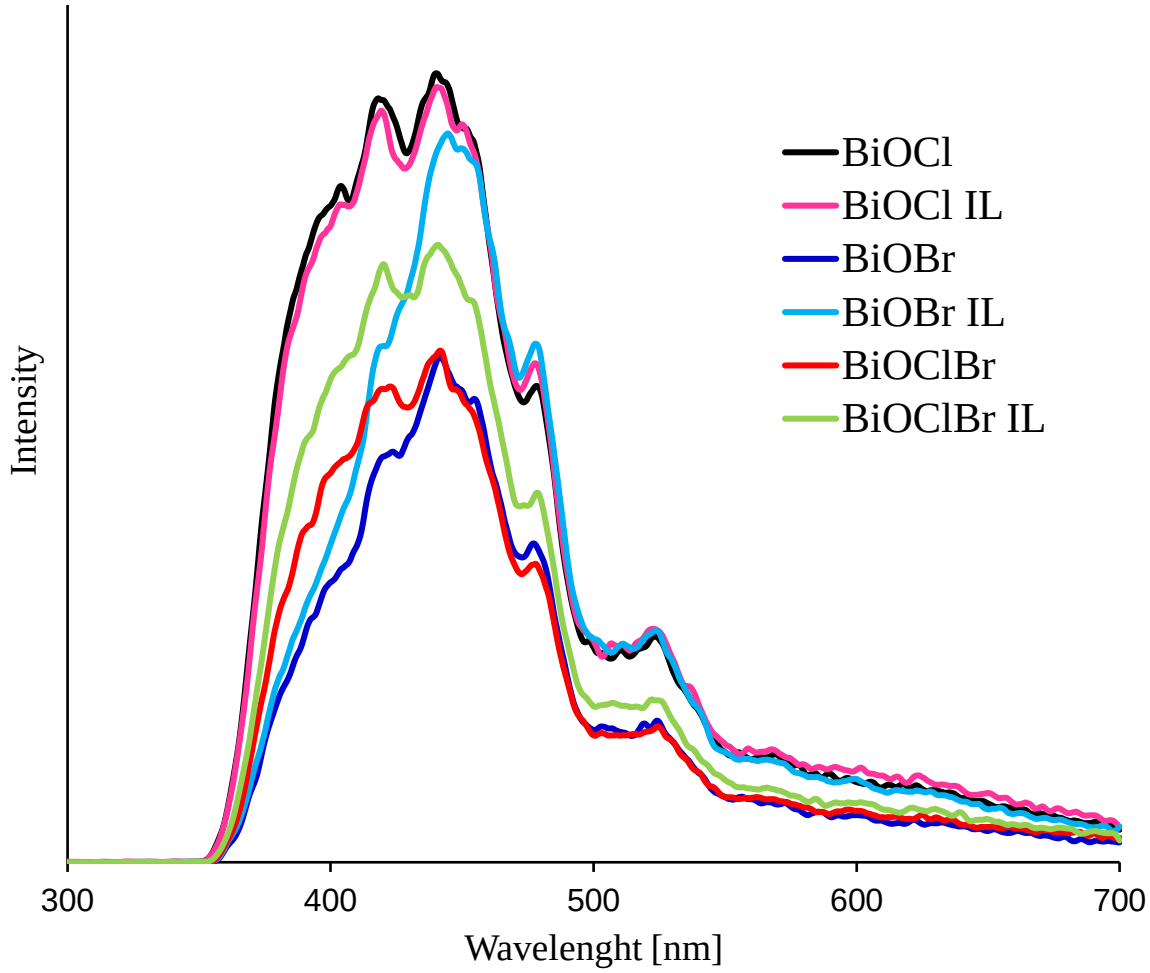

Fig. S4. Photoluminescence spectra of prepared photocatalysts.